Scientia Iranica B (2011) 18 (6), 1237–1245

Sharif University of Technology

Scientia Iranica

Transactions B: Mechanical Engineering

www.sciencedirect.com

Generating a finite element model of the cervical spine: Estimating muscle forces and internal loads

N. Toosizadeh [a], **M. Haghpanahi** [b,*]

[a] *Grado Department of Industrial and Engineering, Virginia Polytechnic Institute and State University (Virginia Tech), Blacksburg, VA, P.O. Box 24060-4943, USA*

[b] *Department of Mechanical Engineering, Iran University of Science and Technology, Tehran, Iran*

Received 24 August 2010; revised 31 July 2011; accepted 17 October 2011

KEYWORDS

Cervical spine;
Finite element approach;
Muscle force;
CT image;
Internal spine loads.

Abstract There are different approaches to Predict the nonlinear moment–rotation relationship and evaluate internal loads and muscle forces of the human cervical spine. In this study a geometrically accurate, nonlinear finite element model of C0–C7 was developed using CT images of the human cervical spine. This model was used to derive the moment–rotation responses of the cervical spine, under physiological moments of 0.33, 0.5, 1.0, 1.5 and 2.0 Nm for flexion/extension in the sagittal plane, lateral bending in the frontal plane and axial rotation. Moreover, the results from the finite element model were used to calculate muscle forces that contribute in equilibrium of the head during rotations in the sagittal and frontal planes. To achieve this, a biomechanical model and the optimization algorithm were used to determine the relationship between required muscle forces and neck angle for the quasi-static condition. Finally, muscle forces were exerted on the finite element model to calculate internal forces. The results showed an excessive increase in internal loads by increasing the angle of rotation in all directions. In conclusion, this study provides evidence of higher cervical spine internal loads in non-neutral head postures, which can be a risk factor for neck pain and arthritis.

1. Introduction

Many researchers have focused on studying the force–deformation behavior of the spine, concentrating more on the lumbar region (e.g. [1,2]). Although cervical spine rotation about all axes is more complex, compared to lumbar regions, there are fewer studies on cervical spine rotation–moment behavior (e.g. [3,4]), and none of them have identified muscle forces and internal loads during these rotations. As such, there is still a need to investigate cervical spine movement with more attention paid to muscle forces and internal loads.

During the last few years, it has been realized that finite element approaches could be more appropriate for determining the role of material properties, or for performing parametric analysis, compared to experimental studies [5]. It is also a non-invasive tool for determining the responses of a normal spine to physiological loadings versus the responses of an injured or a surgically modified spine, and predicting load distributions among different spinal components [5]. Moreover, *In vivo* methods for measuring the internal loads of intervertebral discs (intradiscal pressure) are invasive and costly [6]. Therefore, computational modeling can be utilized to overcome the problems related to internal load measurements.

Multi-segment link models for determining internal loads have been well established in previous research. Many of these studies represent spinal motion segments as ball-and-socket joints with zero stiffness [7]. In more detailed models, elastic behavior from experimental data was defined for each motion segment to account for passive properties [8]. One important limitation of these types of modeling is that they cannot predict force distributions among passive components (i.e., intervertebral discs, ligaments, facet joints and passive muscle components). As such, more geometrically accurate models have been developed with the objective of estimating

* Corresponding author.
E-mail address: mhaghpanahi@yahoo.com (M. Haghpanahi).

doi:10.1016/j.scient.2011.10.002

the stress in each passive component of the spine, and also in providing more accurate estimations of reactive moments during physiological loadings [5].

After defining the model, numerical methods are used to determine force–displacement (stress–strain) behavior. For simple multi-segment link models, numerical computing environments, such as MATLAB or Mathematica, are employed (e.g. [9]). For more complicated models, it is more convenient to use Finite Element (FE) models, implementing commercial software, such as ABAQUS and ANSYS [5].

As such, using the available modeling approaches, it is beneficial to determine the internal loads of the cervical spine at several head angles, to provide a better understanding of the underlying mechanism that can lead to injury or pain. Therefore, the purpose of this study was to estimate forces generated by muscles in different postures of the head, and to use these muscle forces to estimate internal cervical loads. Results from this study provide knowledge about non-neutral head postures as a risk factor of neck disorders.

2. Material and methods

2.1. Geometrical model

In this study, an exact three-dimensional nonlinear finite element model of C0–C7 has been developed. The primary information was obtained from CT images of a 26-year-old female. These images were arranged in a sequential cross-section at 0.6 mm intervals and imported into MIMICS (Materialise Mimics ver. 10.01), in DICOM file format. An image processing step was undertaken to develop bone boundaries, by defining a brightness threshold for detecting bony tissue from surrounding soft tissue. The defined borders for each vertebra were combined together and used to create the outer area of bony tissue. Then, a smoothing procedure was performed on the volume boundaries by replacing each node at a slightly different location. This procedure helps in refining the geometry without any reduction in node (or element) numbers. Subsequently, the surface areas of new volumes of each vertebra were exported to finite element software in IGES file format (Figure 1), with minimum deviation from the original smoothed volume (96% of the surface of the IGES file was within ± 0.03 mm of the smooth anatomical model).

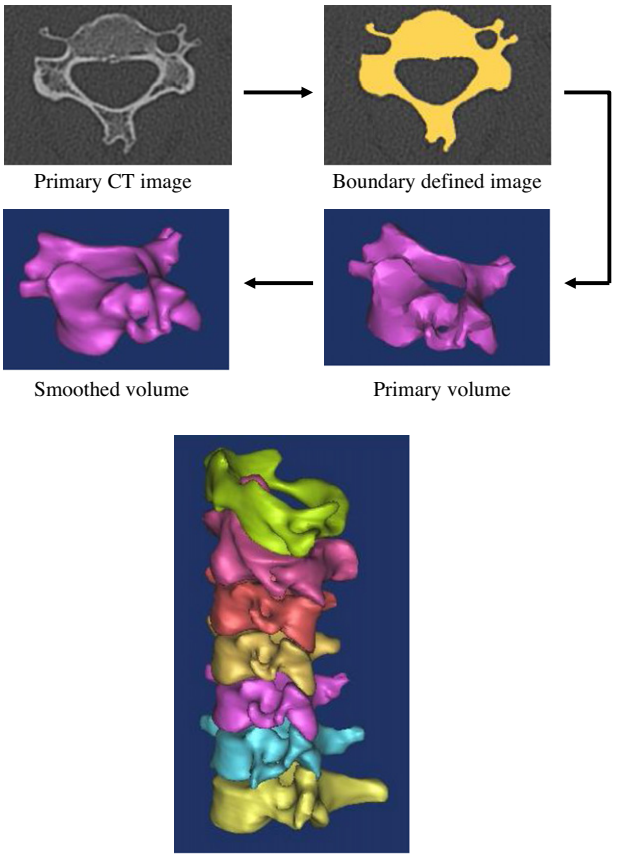

Figure 1: Conversion procedure for developing volumes of bony tissue.

2.2. Finite element model

In this step, the areas of bony tissue were exported to CAE software and used to create soft tissue, including; intervertebral discs, ligaments and joints. The volumes of vertebra body were divided into cortical and cancellous parts, considering an average thickness between 0.4 and 0.5 mm for the cortical region at different levels of the cervical spine [10]. For lower segments of the cervical spine (C2–C7), the intervertebral discs between two vertebral bodies were created. These intervertebral discs were then divided into nucleus pulposus and annulus ground with superimposed fibers. A portion of the nucleus volume was assumed to be about 0.5–0.8 of the disc volume, depending on the disc size [11]. It has been shown that cervical intervertebral discs are not similar to lumbar discs; they lack a concentric annulus fibrosis around their entire perimeter. The cervical annulus is well developed and thickened in the anterior region [12]. Due to this fact, to develop a more precise model, the fibers of each annulus were superimposed like an inverted "V", whose apex points to the axis of rotation of the annulus and the density reduces from the center toward the lateral sides of the annulus. Only a few fibers in the posterior region were represented [12].

Six kinds of element were used to model different parts of the cervical spine (Tables 1 and 2). All joints, involving lower cervical facet joints for C2–C7, Atlanto–Axial and Atlanto–Occipital, were simulated using a contact mechanism. Target and contact elements were considered for contacting parts of each facet, and at the contact points (i.e. nodes with zero or negative distances,) normal and shear forces were estimated using the elastic properties of the bony tissue and friction coefficient, respectively. According to the literature [18], a friction coefficient of 0.01 is appropriate for sliding surfaces. There is a major difference between the contact mechanisms of lower cervical facet joints (C2–C7) and upper cervical joints (C0–C2). The contact mechanisms of the lower cervical facet joints reduce rotational displacement (except for flexion), while the upper cervical joints (Atlanto–Axial and Atlanto–Occipital) contact mechanism restrict the movements of vertebrae and act as boundaries for rotational displacements.

It is difficult to obtain a converged solution in a large sliding simulation if the target surface has sharp convex corners. To avoid such modeling problems in the geometrically accurate model, line and area fillet functions were used on the solid model over sharp corners, and, alternatively, a more refined mesh (higher order elements) was used in the region of abrupt curvature changes. For the Odonoid–Atlas joint, two pairs of contacting structure were used. The anterior contact pair is between the Odonoid process and anterior arc of Atlas; the same structure was used for Odonoid and Transverse ligaments.

Hyper elastic elements were used to model the fluid-like characteristics of the intervertebral disc. This type of modeling provides a uniform distribution of the load in intervertebral discs, as in actual discs [19].

Table 1: Material properties and element types of different components used for finite element model.

Component	Element	Material properties (Elastic modulus in MPa)	Reference
Cortical bone	10 node tetrahedral (solid)	$Exx = 11\,300$, $Gxy = 3800$, $vxy = 0.484$ $Eyy = 11\,300$, $Gyz = 5400$, $vyz = 0.203$ $Ezz = 22\,000$, $Gxz = 5400$, $vxz = 0.203$	[13]
Cancellous bone	10 node tetrahedral (solid)	$Exx = 140$, $Gxy = 48.3$, $vxy = 0.45$ $Eyy = 140$, $Gyz = 48.3$, $vyz = 0.315$ $Ezz = 200$, $Gxz = 48.3$, $vxz = 0.315$	[13]
Posterior element	10 node tetrahedral (solid)	$E = 3500$, $v = 0.3$	[14]
Atlas and skull	10 node tetrahedral (solid)	$E = 2000$, $v = 0.3$	[14]
Annulus ground	10 node tetrahedral (solid)	$C1 = 0.56$, $C2 = 0.14$, $v = 0.45$	[13]
Nucleus pulposus	10 node tetrahedral (hyper elastic solid)	$C1 = 0.12$, $C2 = 0.09$, $v = 0.4999$	[13]
Disc fibers	Tension-only link	$E = 5$ (anterior), $E = 1$ (posterior) $E = 0.1$ (lateral), $v = 0.3$	[15–17]
Alar ligament	10 node tetrahedral (hyper elastic solid)	$E = 5$, $v = 0.3$	[14]
Transverse ligament	10 node tetrahedral (hyper elastic solid)	$E = 20$, $v = 0.3$	[14]
Apical ligament	Tension-only link	$E = 20$, $v = 0.3$	[14]
Capsular ligament of C0–C1	10 node tetrahedral (hyperelastic solid)	$E = 1$, $v = 0.3$	[14]

Table 2: Nonlinear material properties of ligaments.

ALL		PLL		ISL		LF		CL	
Def. (mm)	Force (N)	Def. (mm)	Force (N)	Def. (mm)	Force (N)	Def. (mm)	Force (N)	Def. (mm)	Force (N)
1.4	35.5	1.0	29.0	1.3	16.9	1.9	45.9	1.8	53.6
2.7	64.9	2.0	51.4	2.7	24.4	3.7	82.4	3.9	87.9
4.1	89.7	3.0	71.3	4.0	29.5	5.6	119.6	5.8	109.4
5.4	108.6	4.0	85.8	5.4	32.9	7.5	133.7	7.7	125.8
6.8	119.6	5.0	94.7	6.7	34.9	9.4	147.2	9.7	134.8

Note: ALL: Anterior Longitudinal Ligament; PLL: Posterior Longitudinal Ligament;
ISL: Interspinous Ligament; LF: Ligamentum Flavum; CL: Capsular Ligament [17].

2.3. Material properties

Material properties for each component were established from the literature. The cortical and cancellous bones were considered as orthotropic solids with a specific Young modulus and Poisson ratio for each direction [13]. Other bony tissue (i.e. posterior element of lower vertebrae, Atlas and lower section of skull) has isotropic material properties [14].

The most important component that requires more precise modeling is the intervertebral disc, due to its great influence on lower cervical rotations. The fluid-like behavior of the nucleus substance and annulus ground were simulated using hyper elastic, Mooney–Rivlin material properties, with two parameters (C1, C2). The input data for this model were derived from the strain energy function using the same procedure as previous studies [13,20]. The input parameters for ANSYS solver (ANSYS Inc., Version 10) are C1, C2 and d. The values of C1 and C2 were obtained from the literature [13], and the d parameter was calculated using the following equation for the bulk modulus:

$$d = \frac{6(1-2\nu)}{E}. \quad (1)$$

Conside that ν is the Poisson ratio, and E (elastic modulus) can be estimated using the following equation [4]:

$$E = 6 \times (C1 + C2). \quad (2)$$

The superimposed fibers of the annulus were modeled using nonlinear tension-only links, with 1.2×10^6 cross-section area and initial strain about -0.1. The initial strain was considered to account for pre-stress in the fibers [15]. The number of fibers included in each disc was estimated, based on the fact that 20% of the annulus volume is allocated to these fibers [16].

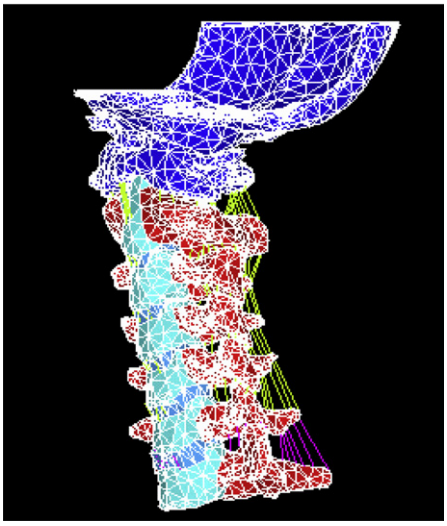

Figure 2: Finite element model of C0–C7.

Ligaments were modeled using nonlinear tension-only springs, and the force–deformation data for each ligament were obtained from the literature [17] (Tables 1 and 2). Among these, the apical ligament was modeled using the nonlinear link element, with a pre-stress of -0.1 strain, according to the literature [14]. The complete FE model is presented in Figure 2.

2.4. Boundary conditions and loading

After completing the model, all segments and the whole cervical spine were subjected to moments of 0.33, 0.5, 1.0, 1.5

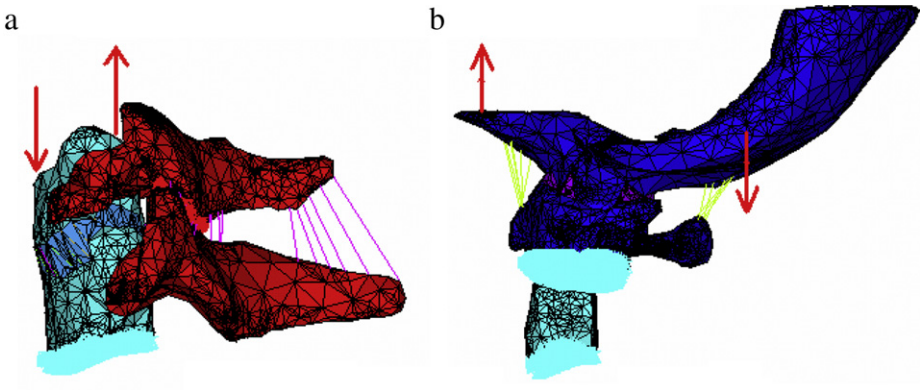

Figure 3: Flexion/extension loading of (a) lower segment, and (b) C0–C2.

Table 3: Origin and insertion data for muscle forces that appear in this study.

Muscle	Insertion X, Y, Z (mm)	Origin X, Y, Z (mm)
Longus Colli	12, 0, 76	7, 0, 0
Longus Capitis	24, 0, 103	12, 10, 76
Splenius Capitis	12, 12, 76	19, 0, 0
Semispinalis Capitis	8, 3, 95	12, 12, 76
Trapezius	−23, 0, 125	−19, 31, 0
Sternocleidomastoid	0, 37, 110	38, 3, 0
Scalenes	12, 12, 76	7, 46, 0

and 2.0 N m, for flexion/extension, lateral bending and axial rotation. For each segment of lower cervical vertebrae (C2–C7), a pair of forces was applied to the top of the upper vertebral body, while the lower vertebra was fixed (Figure 3) to create the external moment. To exert load on the C1–C2 segment, a pair of forces was exerted on the upper facet of Atlas, while the Axis was fixed. For investigating upper cervical (C0–C1) rotations, the rotation of C0–C1–C2 was considered as a whole, due to the coupled movement of C0–C1 and C1–C2 segments [3]. To achieve this, the Axis and the Atlas were fixed and a pair of forces was applied to the skull (Figure 3).

The finite element program, ANSYS (ANSYS Inc., Version 10), was used to analyze the nonlinear behavior of the cervical spine, in response to several loading conditions. For the lower cervical spine, 3–4 substeps, with a total mean value of 15 iterations, were required for convergence. However, the number of substeps for the upper cervical spine was increased to 5 or 6, to prevent highly distorted elements. In these cases, up to 40 iterations were required for convergence.

2.5. Muscle forces calculation

Another goal of this study was to calculate the muscle forces at different head postures. The segmental rotations of the FE model and reactive moments were used as input data. The reactive moments were estimated using the rotation–moment curves from the previous section. A multi-segment link model, including seven pairs of muscle, was used to estimate muscle forces and internal loads. The biomechanical model prepared for this reason was generated in CATIA (SIMULIA Inc., Version 5R15) (Figure 4). Using this software, it was possible to implement the optimization toolbox for calculating muscle forces.

The simple biomechanical model contains joints and links in three-dimensional space. Joint locations were derived from

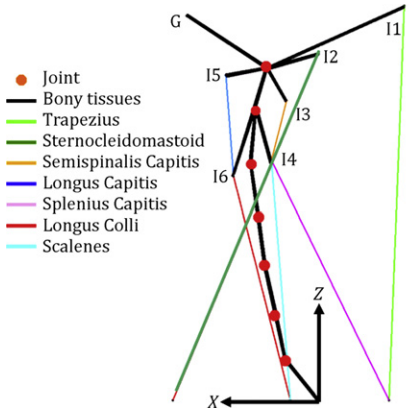

points	X (mm)	Z (mm)
0	0	0
J01	13	106
J12	16	93
J23	17	75
J34	15	58
J45	14	43
J56	11	28
J67	8	13
G	34	122
I1	-23	125
I2	0	110
I3	8	95
I4	12	76
I5	24	103
I6	22	71

Figure 4: Coordinates of joints (J), head centre of gravity (G) and insertion of muscle slips (I) in sagittal plane.

rotation axes in sagittal and frontal planes using previous studies [21]. Each joint was connected to the adjacent one with a link, which represents the vertebra between these two joints. The origin "O" of the coordinate system is on the caudal-dorsal corner of the C7 vertebra, and x, y and z directions of this coordinate system were assumed to be from posterior to anterior, right to left, and inferior to superior, of the human body, respectively. In Figure 4, the model and coordinates of joints are presented. "G" is considered the point of action of the head weight.

In the multi-segment model, for a determined rotation of the neck, the rotation of each segment, and, also, the reactive moment generated by passive soft tissues, were estimated using the FE model and entered into the model. Seven pairs of muscle were considered; their names and their points of insertion and origin are presented in Table 3. The coordinates and physiological cross section area of the muscles were achieved from the literature and scaled for this model [21]. Subsequently, these data were used to estimate muscle forces with the objective of minimizing the reactive moment at each level of the cervical spine. The input parameter for the model was the weight of the head. The equilibrium equation of moments and forces for calculating muscle forces and joint reaction forces are presented here for quasi-static condition [22]:

$$\sum_{i=1}^{n}(F_i \times r_i) + M_{\text{out}} + M_{\text{passive}} = 0, \tag{3}$$

$$\sum_{i=1}^{n} F_i + F_{\text{joint}} = 0. \tag{4}$$

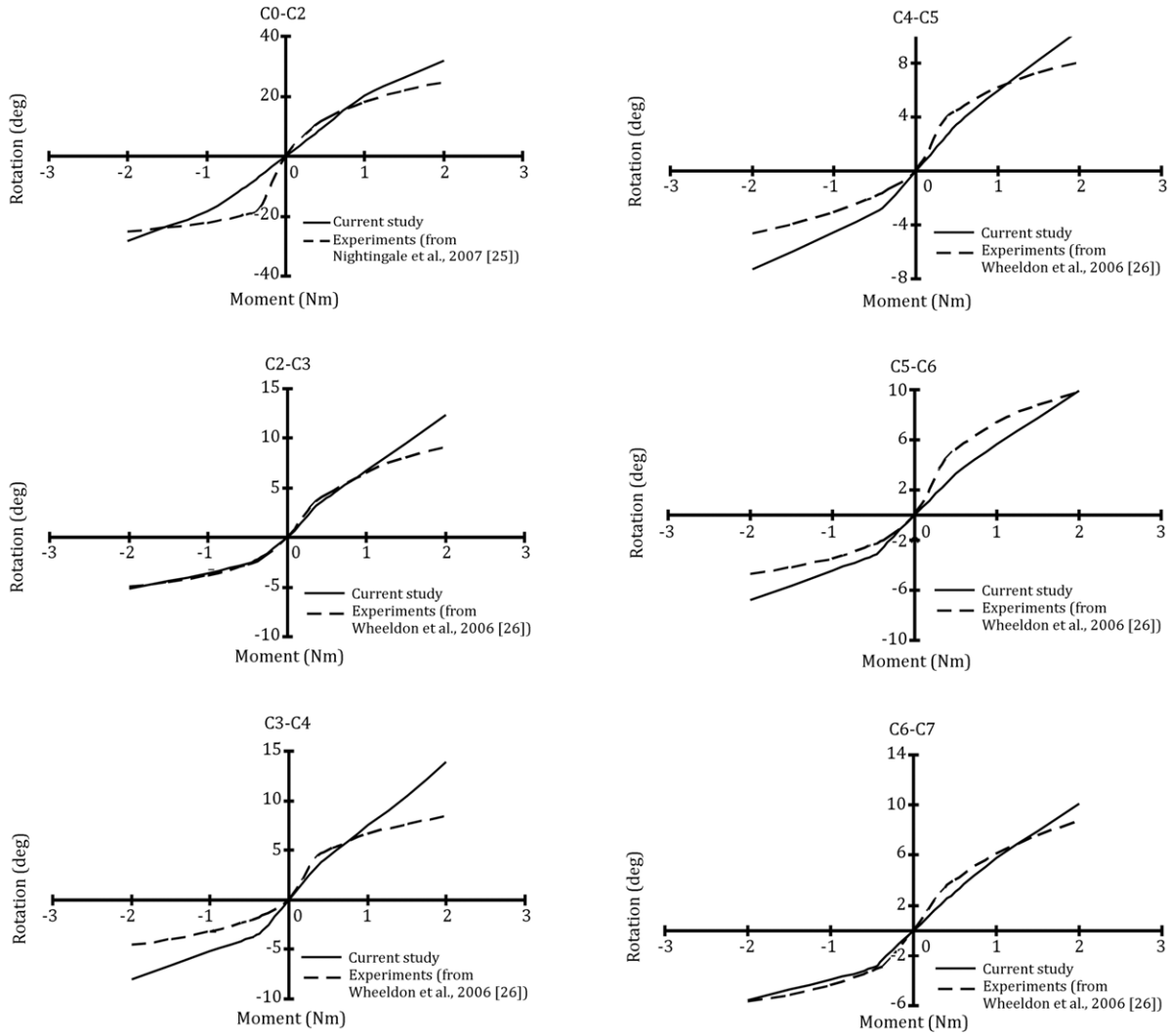

Figure 5: Moment–rotation results for flexion/extension of each motion segment (positive values are for flexion and negative values are for extension).

Here, F_i and r_i are the vectors of muscle force and moment arm, respectively, and "$\times$" stands for vector cross product, M_{out} is the external moment, which is the weight of the head for the C0–C1 joint, M_{passive} is the reactive moment generated by passive tissue, n indicates the number of muscles that contribute to each joint equilibrium, and F_{joint} is the reaction force in the joint.

These equations were solved for each level of the cervical spine. In some cases, where the number of muscles at the joint was more than the equilibrium equations, the system was indeterminate, and an optimization algorithm was used. The method implemented in this study tried to minimize the summation of cubed muscle stress. Thus, the following cost function, as in previous research [23], was employed:

$$\text{Cost} = \sum_{i=1}^{n} \left(\frac{F_i}{A_i} \right)^3. \tag{5}$$

Here, A_i is the physiological cross-section area of the ith muscle. The following constraints were used for the optimization algorithm:

$$\begin{cases} F_i > 0 \\ \dfrac{F_i}{A_i} < S. \end{cases} \tag{6}$$

These constraints were used to indicate that muscles create positive forces, and, also, the fact that the stress of each muscle fascicle should not exceed the permissible stress of S, which was considered to be 100 N cm^{-1} [24]. However, after completing all calculations for different neck rotations, the stress of muscle fascicles never reached this permissible limit. The CATIA (SIMULIA Inc., Version 5R15) optimization toolbox and simulated annealing algorithm were used to solve the problem.

After deriving the magnitudes of muscle forces, the equilibrium of forces in all directions was used to obtain the joint reaction force, F_{joint}, using Eq. (4). The reaction forces of C0–C1 joints took the role of input parameters for the next joint, C1–C2, to calculate the muscle forces connected to the Atlanto–Axial segment. This procedure was carried on for the next muscles in turn, until all muscle forces were calculated.

3. Results

In this study, we have developed an exact three-dimensional finite element model of the cervical spine. This model has both geometrical and material nonlinearity. At the primary step, rotations about axes were calculated and used to validate

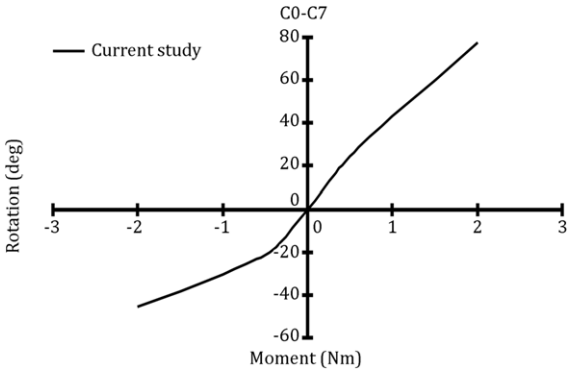

Figure 6: Moment–rotation results for flexion/extension of the whole cervical spine (positive values are for flexion and negative values are for extension).

the model (without muscle forces) using previous studies [14,25,26]. The results were compared for sagittal rotations with *in vitro* experiments performed on cervical motion segments for several magnitudes of external moments [25,26]. However, no experimental result is available for validating the lateral and axial rotations for different loading magnitudes. As such, lateral and axial rotations were compared with experiments [4] and a FE model [14] only for one level of loading (1 N m). Diagrams are presented for five moment magnitudes of 0.33, 0.5, 1.0, 1.5 and 2.0 N m for flexion/extension and lateral bending for each segment and also the entire cervical spine (Figures 5–9).

Another objective of this study was to determine the muscle forces within neck and head rotations, using the developed FE model and the biomechanical model. The responses of 7 muscles against neck rotations for sagittal and lateral bending are presented in Figures 10 and 11 for quasi-static conditions. It is obvious that in sagittal rotations, an equal magnitude of force exists in each fascicle of muscle pairs, so, their values are shown only for one fascicle (left or right). Moreover, Figure 10 shows the responses of left fascicles for right lateral bending. Since the model is sagittally symmetric, the same results are expected for left lateral bending for right muscles. Finally, the equilibrium equation of forces in each segment was used to calculate the joint reaction force. The results for the two upper cervical joints, Atlanto–Occipital and Atlanto–Axial, are presented here (Figure 12). Since the upper cervical spine is the most susceptible to injury [27], only results of this region were considered.

4. Discussions

It can be seen in the diagrams that for the lower cervical spine, flexion/extension curves are asymmetric with greater magnitudes of rotational stiffness in extension compared to flexion. The same results have been reported by previous studies regarding the differences in rotational stiffnesses in flexion and extension [4,25,26]. Also, previous researchers demonstrated that soft tissue has nonlinear force–deformation responses, and, in physiological ranges, stiffness increases with external force or moment [28,29]. The nonlinear material properties were established in this study using nonlinear force–deformation tables for ligaments, and pre-stress for disc fibers and upper cervical ligaments. Furthermore, facet joints and all upper cervical joints can cause an increase in rotational stiffness, especially in higher magnitudes of external moments. It is apparent from flexion/extension and lateral bending figures of the lower cervical spine that a sudden drop in curve slopes

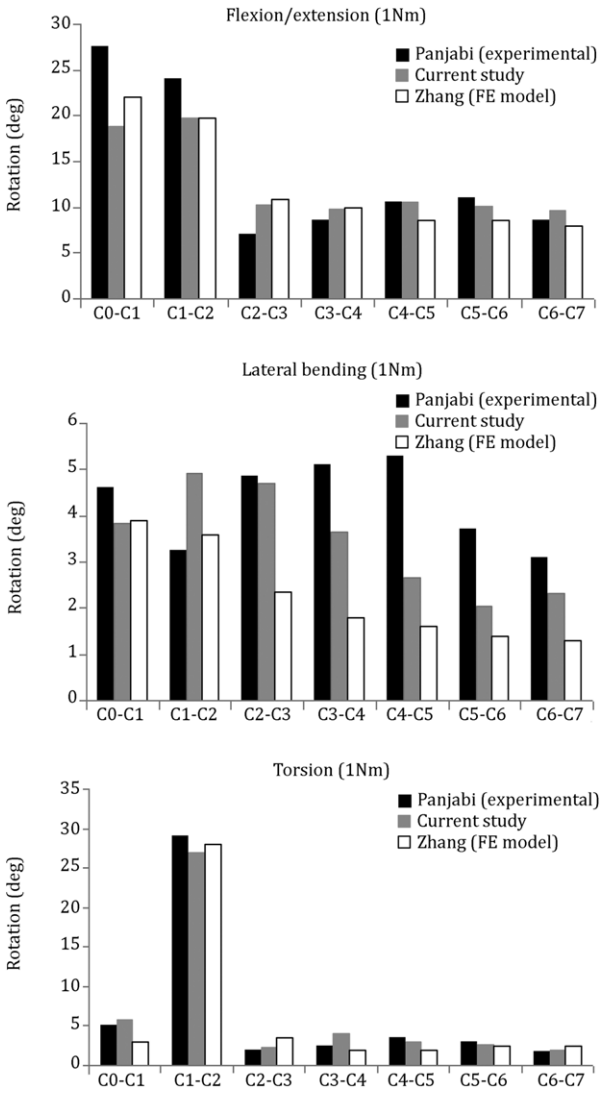

Figure 7: Results for 1 N m moment for flexion/extension (sum of flexion and extension), right lateral bending and right axial rotation.

occurred between 0.5 and 1.0 N m moments, due to the rise in stiffness of disc fibers. Also, a continuous increase in stiffness occurred because of the nonlinear material properties of ligaments, facet joints and, also, the geometrical nonlinearity.

It is impossible to calculate muscle forces in a static condition, using in vivo experiments, such as electromyography (EMG). Moreover, *in vivo* methods for measuring the internal spine loads are invasive and costly. Therefore, modeling approaches have been introduced for estimating muscle forces and internal loads. It should be noted that the calculated muscle forces here are not active dynamic forces required for neck movements, and all calculations were performed for quasi-static conditions. Results show that posterior muscles, including Trapezius, Sternocleidomastoid, Splenius Capitis and Scalenes, have a more significant role to play in head and neck equilibrium in flexed postures. On the other hand, Longus Colli, which is an anterior muscle, has a greater magnitude of generated force in extension. Semispinalis Capitis and Longus Capitis, which are positioned between other fascicles, did not obey this rule. It can be concluded that these muscles have a moderating role in reducing lower joint reaction forces and a stabilizing function.

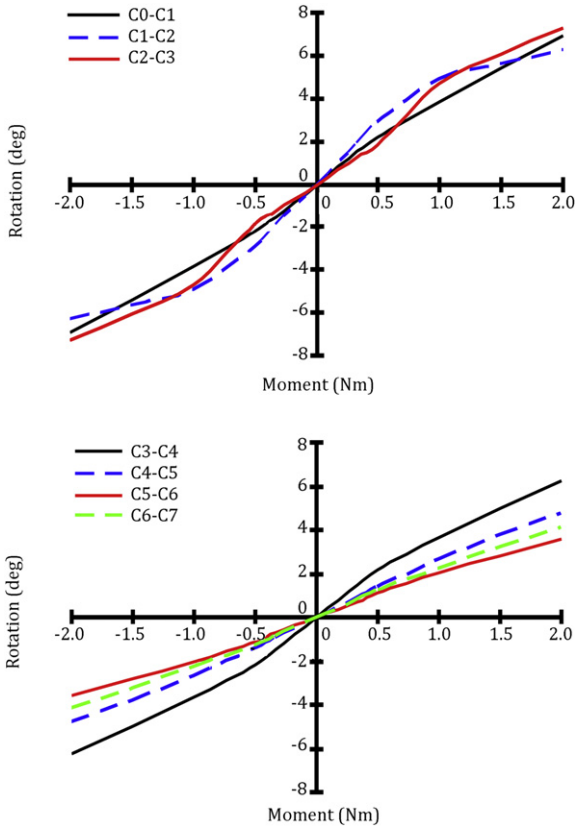

Figure 8: Moment–rotation results for lateral bending of each motion segment (positive values are for right bending and negative values are for left bending).

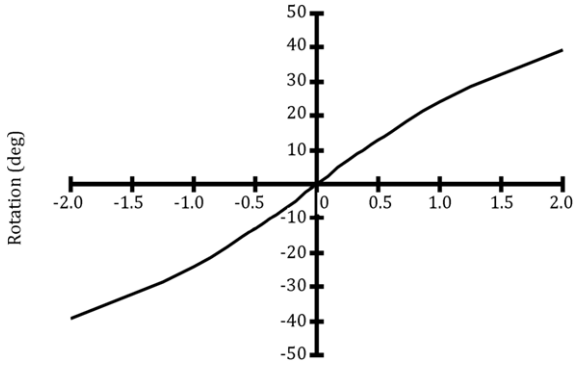

Figure 9: Moment–rotation results for lateral bending of the whole cervical spine (positive values are for right bending and negative values are for left bending).

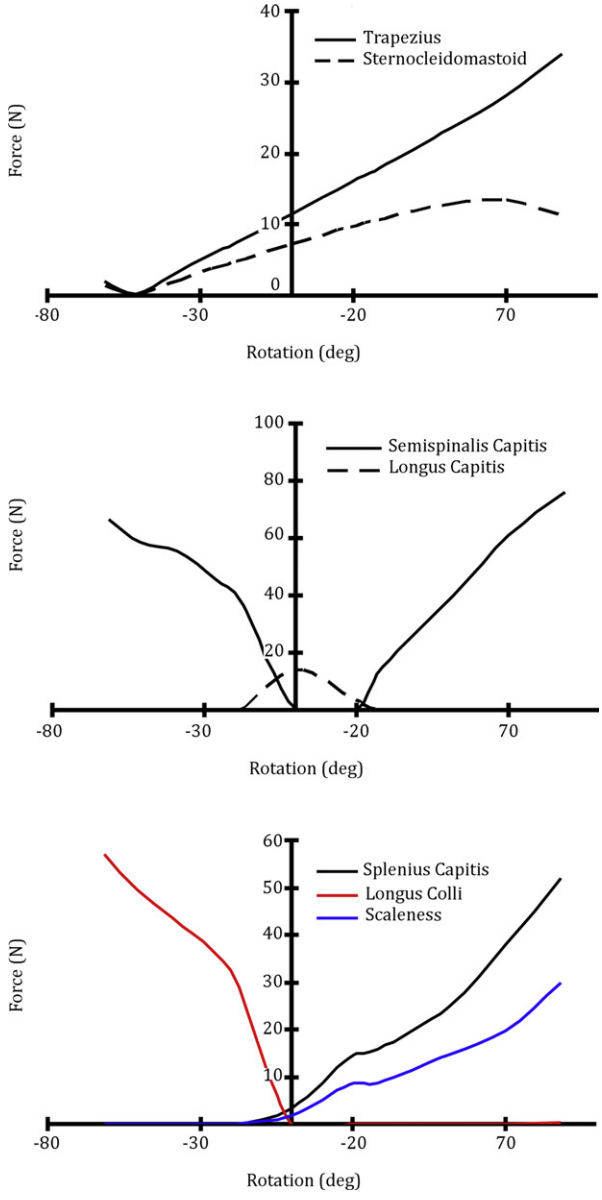

Figure 10: Force–rotation results for muscles in flexion/extension (positive values are for flexion and negative values are for extension).

For lateral bending, a different mechanism can be seen, due to the fact that each slip of muscle pairs creates a unique force in different postures. For flexion/extension, only the equilibrium of moments about the "y" axis should be fulfilled, but, in lateral rotation, the equilibrium should be considered about all three axes. Therefore, it is difficult to predict muscle forces at different positions of the head. According to Figure 11, when the neck rotates to the right side, the most effective muscles on the left side that have a significant role to play in equilibrium are Sternocleidomastoid, Splenius Capitis and Scalenes. On the other hand, for right lateral bending, right slips of Trapezius, Semispinalis Capitis and Longus Capitis create a large magnitude of forces. Because of the position of the Longus Colli in the sagittal plane, there is an equal response in both left and right lateral bending (Figure 11). Also, it is apparent that the largest force was created by the Semispinalis Capitis and Splenius Capitis, during lateral bending, which reached 160 N. Another interesting observation is the ineffective role of Longus Capitis in flexion and extension. In the neutral posture of the head, this muscle was active, but, the magnitude of the Longus Capitis force became zero as the neck flexed or extended.

In Figure 12, the magnitudes of Atlanto–Occipital and Atlanto–Axial joint reaction forces are presented. The average values of these forces were 83 and 60 N for Atlanto–Occipital and Atlanto–Axial joints during flexion/extension, respectively, and 98 and 107 N for lateral bending. This states that a higher reaction force was generated in the Atlanto–Occipital joint in sagittal bending, and for lateral bending, the magnitude of the reaction forces of the Atlanto–Axial joint became larger. In Figure 12, when there is a lateral of bending more than 20°, the value of reaction forces in the Atlanto–Axial joint increases suddenly, up to 240 N. This suggests an increase in internal

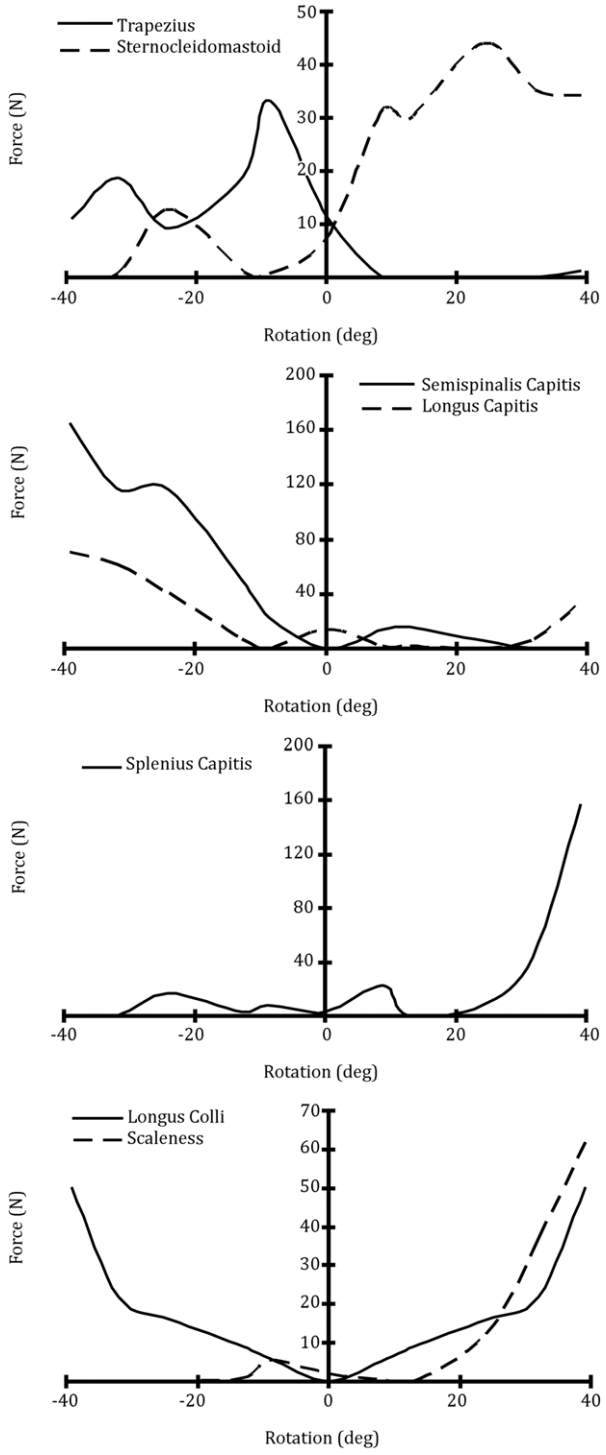

Figure 11: Force–rotation results for muscles in lateral bending (positive values are for right bending and negative values are for left bending).

load magnitudes in larger rotational displacements, especially in lateral bending.

One limitation of the current study is related to validating the muscle force estimations and also internal forces. Rotation–moment properties of the cervical spine motion segments were evaluated using both experimental studies and previously developed FE models. However, because of limitations in experimental studies, the muscle force and internal load estimations

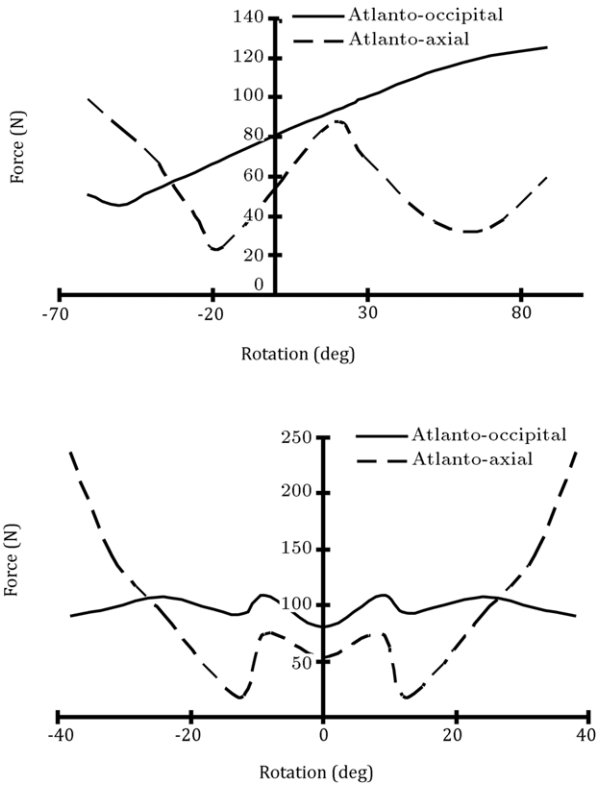

Figure 12: Force–rotation diagrams for Atlanto–Occipital and Atlanto–Axial joints reaction forces. (a) Reaction force during flexion (positive rotations) and extension (negative rotations); and (b) reaction force during lateral bending for right (positive rotations) and left (negative rotations) bending.

were not evaluated. The force calculation method used here has been validated for the lumbar spine, and, therefore, estimated muscle forces in this study are assumed to provide a reasonable prediction of actual muscle activities. However, more accurate estimations can be performed in future studies by comparing current results with other acceptable methods, such as EMG-assisted or *in vivo* methods.

5. Conclusions

A complete model of the cervical spine, including all motion segments and head, was developed in this study. After validating this model with previous studies, it was used to estimate muscle forces and internal loads. According to predictions, more risk of tissue injury exists in the lateral bending of the head compared to flexion or extension. Moreover, the estimated internal forces were smaller than the failure tolerance [30]. However, due to repetition and prolonged bending (and, consequently, reduction in tissue tolerance) or inflammation of muscles and ligaments, these exposures might lead to injury. As such, more investigations are required to evaluate the effect of different types of tissue injury and also prolonged/repetitive loading on internal spine loads.

References

[1] Marras, W.S. and Sommerich, C.M. "A three-dimensional motion model of loads on the lumbar spine: I. Model structure", *Human Factors*, 33, pp. 123–137 (1991).

[2] Mcgill, S.M. "The biomechanics of low back injury: implication on current practice in industry and the clinic", *Journal of Biomechanics*, 30(5), pp. 465–475 (1996).

[3] Ishii, T., Mukai, Y., Hosono, N., Sakaura, H., Fujii, R., Nakajima, Y., Tamura, S., Sugamoto, K. and Yoshikawa, H. "Kinematics of the subaxial cervical spine in rotation in vivo three-dimensional analysis", *Spine*, 29(24), pp. 2826–2831 (2004).
[4] Panjabi, M., Dvorak, J., Duranceau, J., Yamamoto, I., Gerber, M., Rauschning, W. and Bueff, H.U. "Three-dimensional movements of the upper cervical spine", *Spine*, 13(7), pp. 726–730 (1988).
[5] Teo, E.C. and Ng, H.W. "Evaluation of the role of ligaments, facets and disc nucleus in lower cervical spine under compression and sagittal moments using finite element method", *Medical Engineering & Physics*, 23(3), pp. 155–164 (2001).
[6] Wilke, H.-J., Neef, P., Hinz, B., Seidel, H. and Claes, L. "Intradiscal pressure together with anthropometric data: a data set for the validation of models", *Clinical Biomechanics*, 1(1), pp. S111–S126 (2001).
[7] Plamondon, A., Gagnon, M. and Desjardins, P. "Validation of two 3-D segment models to calculate the net reaction forces and moments at the L(5)/S(1) joint in lifting", *Clinical Biomechanics (Bristol, Avon)*, 11(2), pp. 101–110 (1996).
[8] Stokes, I.A.F. and Gardner-morse, M. "Lumbar spine maximum efforts and muscle recruitment patterns predicted by a model with multijoint muscles and joint stiffness", *Journal of Biomechanics*, 28(2), pp. 173–186 (1995).
[9] Feng, C.-K., Chen, C.-S., Chen, C.-H., Lee, S.-J., Liu, C.-L., Lee, Y.-E. and M.-W., Tsai "A 3D mathematical model to predict spinal joint forces for a child with spina bifida", *Gait & Posture*, 30(3), pp. 388–390 (2009).
[10] Ritzel, H., Amling, M., Pösl, M., Hahn, M. and Delling, G. "The thickness of human vertebral cortical bone and its changes in aging and osteoporosis: a histomorphometric analysis of the complete spinal column from thirty-seven autopsy specimens", *Journal of Bone and Mineral Research: the Official Journal of the American Society for Bone and Mineral Research*, 12(1), pp. 89–95 (1997).
[11] Yoganandan, N., Kumaresan, S. and Pintar, F.A. "Biomechanics of the cervical spine. Part 2. Cervical spine soft tissue responses and biomechanical modeling", *Clinical Biomechanics*, 16(1), pp. 1–27 (2001).
[12] Bogduk, N. and Mercer, S. "Biomechanics of the cervical spine. I: normal kinematics", *Clinical Biomechanics (Bristol, Avon)*, 15(9), pp. 633–648 (2000).
[13] Schmidt, H., Heuer, F., Simon, U., Kettler, A., Rohlmann, A., Claes, L. and H.-J., Wilke "Application of a new calibration method for a three-dimensional finite element model of a human lumbar annulus fibrosus", *Clinical Biomechanics*, 21(4), pp. 337–344 (2006).
[14] Zhang, Q.H., Teo, E.C., Ng, H.W. and Lee, V.S. "Finite element analysis of moment–rotation relationships for human cervical spine", *Journal of Biomechanics*, 39(1), pp. 189–193 (2006).
[15] Maurel, N., Lavaste, F. and Skalli, W. "A three-dimensional parameterized finite element model of the lower cervical spine. Study of the influence of the posterior articular facets", *Journal of Biomechanics*, 30(9), pp. 921–931 (1997).
[16] Ha, S.K. "Finite element modeling of multi-level cervical spinal segments (C3–C6) and biomechanical analysis of an elastomer-type prosthetic disc", *Medical Engineering & Physics*, 28(6), pp. 534–541 (2006).
[17] Kumaresan, S., Yoganandan, N., Pintar, F.A. and Maiman, D.J. "Finite element modeling of the cervical spine: role of intervertebral disc under axial and eccentric loads", *Medical Engineering & Physics*, 21(10), pp. 689–700 (1999).
[18] Kumaresan, S., Yoganandan, N. and Pintar, F.A. "Finite element modeling approaches of human cervical spine facet joint capsule", *Journal of Biomechanics*, 31(4), pp. 371–376 (1998).
[19] Iatridis, J.C., Weidenbaum, M., Setton, L.A. and Mow, V.C. "Is the nucleus pulposus a solid or a fluid? mechanical behaviors of the nucleus pulposus of the human intervertebral disc", *Spine*, 21(10), pp. 1174–1184 (1996).
[20] Gagnon, M.W., Hubert, P., Semler, C., Païdoussis, P.M., Vezina, M. and Lavoie, D. "Hyperelastic modeling of rubber in commercial finite element software (ANSYSTM)", SAMPE 2006, Long Beach, CA, United States, p. 15 (2006).
[21] Snijders, C.J., Hoek Van Dijke, G.A. and Roosch, E.R. "A biomechanical model for the analysis of the cervical spine in static postures", *Journal of Biomechanics*, 24(9), pp. 783–792 (1991).
[22] Ezquerro, F., Simón, A., Prado, M. and Pérez, A. "Combination of finite element modeling and optimization for the study of lumbar spine biomechanics considering the 3D thorax-pelvis orientation", *Medical Engineering & Physics*, 26(1), pp. 11–22 (2004).
[23] Bazrgari, B., Shirazi-Adl, A., Trottier, M. and Mathieu, P. "Computation of trunk equilibrium and stability in free flexion-extension movements at different velocities", *Journal of Biomechanics*, 41(4), pp. 412–421 (2008).
[24] Skalli, W. "Personalized cervical muscles 3D geometry and inter-individual volume variations", *Congres de la Societe de Biomecanique*, 153, pp. 8–10 (2004).
[25] Nightingale, R.W., Chancey, V.C., Ottaviano, D., Luck, J.F., Tran, L., Prange, M. and Myers, B.S. "Flexion and extension structural properties and strengths for male cervical spine segments", *Journal of Biomechanics*, 40(3), pp. 535–542 (2007).
[26] Wheeldon, J.A., Pintar, F.A., Knowles, S. and Yoganandan, N. "Experimental flexion/extension data corridors for validation of finite element models of the young, normal cervical spine", *Journal of Biomechanics*, 39(2), pp. 375–380 (2006).
[27] Nuckley, D.J., Hertsted, S.M., Ku, G.S., Eck, M.P. and Ching, R.P. "Compressive tolerance of the maturing cervical spine", *Stapp Car Crash Journal*, 46, pp. 431–440 (2002).
[28] Wagner, D.R. and Lotz, J.C. "Theoretical model and experimental results for the nonlinear elastic behavior of human annulus fibrosus", *Journal of Orthopaedic Research: Official Publication of the Orthopaedic Research Society*, 22(4), pp. 901–909 (2004).
[29] Weiss, J.A., Gardiner, J.C. and Bonifasi-Lista, C. "Ligament material behavior is nonlinear, viscoelastic and rate-independent under shear loading", *Journal of Biomechanics*, 35(7), pp. 943–950 (2002).
[30] Pintar, F.A., Yoganandan, N. and Voo, L. "Effect of age and loading rate on human cervical spine injury threshold", *Spine*, 23(18), pp. 1957–1962 (1998).

Nima Toosizadeh obtained his B.S. degree in Mechanical Engineering from Amirkabir University of Technology (Tehran Polytechnic), Iran, and his M.S. degree in Biomechanics from Iran University of Science and Technology. He is, currently, a Ph.D. degree student of Industrial and Systems Engineering, and has been studying at Virginia Polytechnic Institute and State University (Virginia Tech) since spring, 2009. His activities are chiefly related to models of spine kinetics and kinematics, occupational biomechanics, finite element modeling, measuring and modeling of soft tissue viscoelastic behavior, static and dynamic measurement and analysis of human movement and human gait modeling.

Mohammad Haghpanahi is Associate Professor in the Mechanical Engineering of Iran University of Science and Technology since 1986. His teaching interests are finite element analysis of linear and nonlinear systems, continuum mechanics, vibration of continuous systems, machine design, strength of material. Also His research interests are welding, finite element stress analysis of systems with nonlinearities (geometrical and material), modal analysis, spine biomechanics, elastography and hyperthermia in soft tissues.